Journal of Materials Chemistry C

ROYAL SOCIETY OF CHEMISTRY

PAPER

View Article Online
View Journal | View Issue

Cite this: *J. Mater. Chem. C*, 2021, **9**, 4927

Engineering donor–acceptor conjugated polymers for high-performance and fast-response organic electrochemical transistors†

Hanyu Jia, ‡[ab] Zhen Huang, ‡[c] Peiyun Li, ‡[a] Song Zhang, [d] Yunfei Wang, [d] Jie-Yu Wang,[c] Xiaodan Gu [d] and Ting Lei *[ae]

Received 29th January 2021,
Accepted 15th March 2021

DOI: 10.1039/d1tc00440a

rsc.li/materials-c

To date, high-performance organic electrochemical transistors (OECTs) have mostly been based on polythiophene systems. Donor–acceptor (D–A) conjugated polymers are expected to be promising materials for OECTs owing to their high mobility and comparatively low crystallinity (good for ion diffusion). However, the OECT performance of D–A polymers lags far behind that of the polythiophenes. Here we synergistically engineered the backbone and side chain of a series of diketopyrrolopyrrole (DPP)-based D–A polymers and found that redox potential, molecular weight, solution processability, and film microstructures all have a severe impact on their performance. After systematic engineering, P(bgDPP-MeOT2) exhibited the best figure-of-merit (μC^*) of 225 F cm^{-1} V^{-1} s^{-1}, amongst the highest performance of the reported D–A polymers. Besides, the DPP polymers exhibited high hole mobility of over 1.6 cm^2 V^{-1} s^{-1}, leading to fast response OECTs with a record low turn-off response time of 30 μs. The polymer also exhibited good operation stability with a current retention of 98.8% over 700 electrochemical switching cycles. This work reveals the complexity and systematicness in the development of D–A polymer based high-performance OECTs.

Introduction

Organic mixed ionic and electronic conductors (OMIECs), have been used for a wide range of applications including sensors, optoelectronics, bioelectronics, and energy storage devices.[1,2] Among these devices, organic electrochemical transistors (OECTs) are particularly attractive because they couple both ionic and electronic inputs to modulate the channel conductance of a transistor in an aqueous environment. OECTs have demonstrated their utility in transducing and amplifying low amplitude electrophysiological signals,[3–5] metabolite sensors,[6–8] and neuromorphic computing.[9,10]

To evaluate the performance of an OECT material, the following equation is often used (eqn (1)):[4,11,12]

$$g_m = \frac{\partial I_{DS}}{\partial V_{GS}} = \frac{W}{L} \cdot d \cdot \mu \cdot C^* \cdot (V_{Th} - V_{GS}) \quad (1)$$

where g_m is the transconductance in the saturation regime; I_{DS} is the drain current; L, W, d are the channel length, width, and film thickness, respectively; μ is the charge carrier mobility; C^* is the volumetric capacitance, V_{Th} is the threshold voltage, and V_{GS} is the applied gate voltage. Recently, the product of μ and C^* has been proposed to benchmark an OECT material and to realize a better comparison between different materials.[11] μC^* is the intrinsic property of a material independent of device geometry and bias conditions. Usually, the higher the μC^* of the channel material, the more excellent the performance of the OECT.

Response speed is another important factor of an OECT device, which is particularly important for applications, such as real-time neural signal amplification, high-quality bio-interfacing transmission, and neuromorphic simulations.[4,13,14] Notably, the response speed of OECTs is usually slower than that of organic field-effect transistors (OFETs) because both polymer swelling and ion diffusion are involved,[15] limiting their

[a] *Key Laboratory of Polymer Chemistry and Physics of Ministry of Education, School of Materials Science and Engineering, Peking University, Beijing 100871, China. E-mail: tinglei@pku.edu.cn*
[b] *School of Materials Science and Engineering, The Key Laboratory of Material Processing and Mold of Ministry of Education, Henan Key Laboratory of Advanced Nylon Materials and Application, Zhengzhou University, Zhengzhou 450001, China*
[c] *College of Chemistry and Molecular Engineering, Peking University, Beijing 100871, China*
[d] *School of Polymer Science and Engineering, The University of Southern Mississippi, Hattiesburg, MS 39406, USA*
[e] *Beijing Key Laboratory for Magnetoelectric Materials and Devices, Peking University, Beijing 100871, China*

† Electronic supplementary information (ESI) available. See DOI: 10.1039/d1tc00440a

‡ These authors contribute equally to this work.

applications in fast signal capturing.[16] Therefore, conjugated polymers with high charge carrier mobility are desired for OECTs.

Recently, several thiophene-based conjugated polymers functionalized with ethylene glycol (EG) side chains, *e.g.* P(g2T-TT),[17] P(g2T-T),[18] and P(g2T2-g4T2)[19] have been developed. These polythiophene systems have exhibited a high μC^* of over 100 F cm^{-1} V^{-1} s^{-1}, thus outperforming the conventional materials poly(3,4-ethylenedioxythiophene):poly(styrenesulfonate) (PEDOT:PSS)[11] and their derivatives, *e.g.* Crys-P,[20] in many aspects. However, the backbone and the corresponding energy level of polythiophene systems are facing the problem of limited tunability, leaving no room for the development of n-type conjugated polymers, which hampers the application of OECTs in CMOS-like logic circuit and bioelectronics.[21,22]

Donor–acceptor (D–A) conjugated polymers have made great advances in the past few years.[23–25] The good backbone planarity, low energetic disorder, and strong interchain interactions make D–A polymers successfully realize high charge carrier mobility with low crystallinity or near amorphous films.[26] Recently, several D–A polymers, using isoindigo (IID), naphthalenediimide (NDI), and pyridine-flanked diketopyrrolopyrrole (PyDPP) building blocks, have been developed as the OECT channel materials.[27–29] These materials have shown a huge potential for OECTs, including (i) diverse structures that provide vast exploration space and possibilities and (ii) large regulation range of the frontier orbital energy level to achieve n-type polymers and stable device operation.[30] Unfortunately, these D–A polymers only exhibited moderate OECT performance with inferior μC^* (<10 F cm^{-1} V^{-1} s^{-1}) and slow temporal response, which have not shown the full potential of D–A polymers. Very recently, McCulloch *et al.* reported several diketopyrrolopyrrole (DPP) polymers for OECTs.[31] In the study, they demonstrated that P(gDPP-T2) exhibited the best OECT performance due to good polaron delocalization. This result is very encouraging because they demonstrate the potential of D–A polymers for high performance OECTs, whereas donor engineering is the only influencing factor that was investigated. However, in our long-term research, we systematically engineered the backbone, side-chain and processing methods *etc.* and found that these factors are interactive in D–A polymers, which is more complex than usually expected.

The structure–property relationship in conjugated polymers is a complicated issue and needs to be fully explored. Here, we report a series of diketopyrrolopyrrole (DPP)-based D–A polymers copolymerized with various donor moieties and grafted with linear or branched EG side chains. Through donor, side chain, polymerization method, and processing solvent engineering, we successfully realized high figure-of-merit OECTs with μC^* of up to 225 F cm^{-1} V^{-1} s^{-1}, high carrier mobility over 1.6 cm^2 V^{-1} s^{-1}, and fast temporal response. Each factor plays a crucial part and shows a great impact on the performance of OECTs.

Results and discussion

Three donor moieties with increased electron-donating properties, *e.g.* thiophene, 2,2′-bithiophene, and 3,3′-methoxy-2,2′-bithiophene (Scheme 1), were used as the donor to tune the highest occupied molecular orbital (HOMO) energy level of the polymers. Similar to previous studies,[17,18] triethylene glycol (R_1 in Scheme 1) was first used as the side chain. However, the strong π–π stacking interactions of the DPP moiety made all the polymers insoluble after polymerization. Therefore, branched EG side chains (R_2 in Scheme 1) were employed to increase the solubility of the polymer. We found that when the monomer was grafted with branched EG chains, Stille polymerization using $Pd_2(dba)_3$/P(*o*-tolyl)$_3$ as the catalyst only yielded oligomers and unreacted monomers. D–A polymers grafted with EG chains synthesized with similar polymerization conditions in the literature only showed low molecular weights (<10 kDa),[27] consistent with our results. After several trials, we found that $Pd(PPh_3)_4$ or $Pd(PPh_3)_2Cl_2$ can provide significantly higher molecular weight

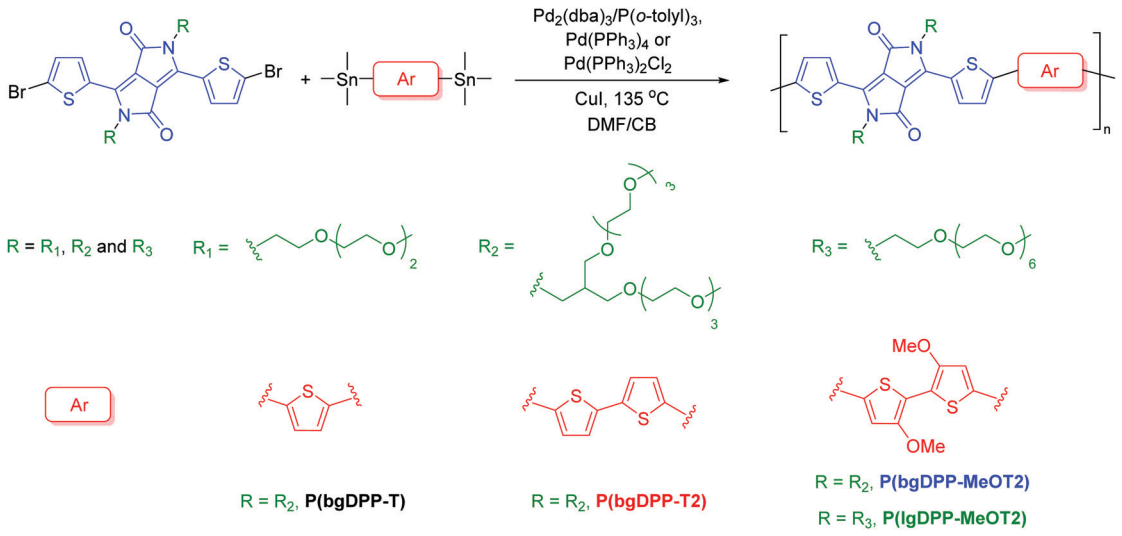

Scheme 1 Synthesis and chemical structures of DPP based D–A polymers with different donor moieties and grafted with linear or branched EG side chains.

polymers when using *N*,*N*-dimethylformamide (DMF) as the solvent. We hypothesize that the branched EG side chains may inhibit the catalytic activity of $Pd_2(dba)_3$/P(*o*-tolyl)$_3$, probably due to the bulky PEG as the side chains for Stille cross-coupling reactions.[32] To prevent the precipitation of polymers caused by the decreased polymer solubility in DMF, we used a DMF/chlorobenzene 1 : 1 mixture as the solvent. CuI was added to accelerate the rate of transmetalation for higher molecular weight.[32] We observed that the reaction rate significantly increased as the reaction mixture turned into deep blue in a few minutes, and higher molecular weight polymers could be obtained.

Unlike D–A polymers with alkyl side chains, whose molecular weight can be evaluated using high-temperature GPC (HT GPC, usually 150 °C) and 1,2,4-tricholorobenzene (TCB) as the eluent,[25] these polymers did not show reasonable molecular weight or observable signals using HT GPC. This is probably due to the hydrophilic side chains since we observed that even though the polymers are visually dissolved in common aromatic or chlorinated solvents (*e.g.* *o*-DCB and chloroform), after spin-coating, the polymer films showed large chunks (Fig. S1, ESI†). After trying several eluents, we found that polar solvent hexafluoroisopropanol (HFIP) is a good eluent for molecular weight characterization. When using chloroform as the eluent, the polymers showed high molecular weights with M_n in the range of 61–71 kDa (Fig. S2, ESI†). In contrast, the molecular weights measured using HFIP as the eluent render the M_n of DPP polymers falling into the range of 26–30 kDa, suggesting the disaggregation of the polymers in HFIP (Table S1 and Fig. S3, ESI†). These molecular weight values are comparable to their alkyl side chain counterparts.[33] In prior studies, McCulloch *et al.* also found that copolymers with a glycol chain form bimodular elution using chlorobenzene as eluents in GPC measurements due to aggregation.[34] Therefore, the molecular weight data of OECT polymers cannot be given in many papers.[31] Our research provides an effective and reliable molecular weight characterization method for polymers with EG chains.

To understand the side-chain effects (linear *vs.* branched), a longer linear EG side chain (R_3 in Scheme 1) with the same number of EG segments ($-OCH_2CH_2-$) was used, yielding polymer P(lgDPP-MeOT2). The long linear glycol chains cannot provide enough solubility and only part of the polymers was Soxhlet extracted, giving a low yield of 26%. All the polymers exhibited good thermal stability with the decomposition temperature of over 300 °C (Fig. S4, ESI†).

The optoelectronic properties of the polymers were evaluated using UV-Vis-NIR absorption spectroscopy and cyclic voltammetry (CV). The polymers exhibit a gradual red-shift of absorption maxima when replacing the donor moiety with a stronger electron-donating unit, either in the solution, or film, or annealed film (Fig. 1a and Fig. S5, ESI†). DPP polymers containing the most electron-rich donor, namely MeOT2, including P(lgDPP-MeOT2), and P(bgDPP-MeOT2), exhibited a smaller bandgap than P(bgDPP-T) and P(bgDPP-T2) (Table S2, ESI†). Therefore, introducing a stronger electron-donating moiety (MeOT2) can remarkably lower the bandgap, largely due to increased HOMO energy levels and enhanced intrachain charge transfer. The higher HOMO levels also make P(lgDPP-MeOT2) and P(bgDPP-MeOT2) more susceptible to oxidation in HFIP solution,

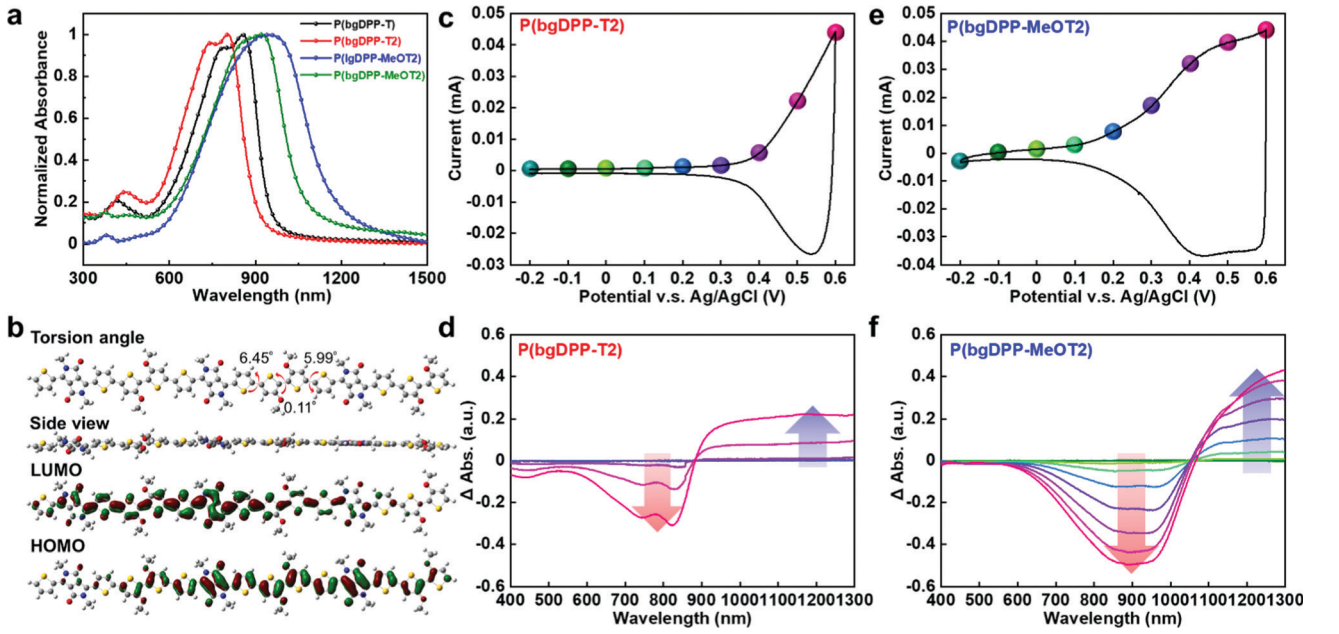

Fig. 1 (a) UV-Vis-NIR spectra of spin-coated films of the four polymers after annealing. (b) DFT-optimized geometries and molecular frontier orbitals of the trimer of DPP-MeOT2. Calculations were performed at the B3LYP/6-311G(d,p) level. Side chains were replaced with methyl groups to simplify the calculations. (c and e) Cyclic voltammograms and (d and f) differential electrochemical absorption spectra of DPP polymers with branched EG side chains. The color-coding UV-Vis-NIR spectra indicate the applied voltage, ranging from −0.2 V to 0.6 V with an interval of 0.1 V. The variation trends of spectra are highlighted with arrows.

which induced a rising of polaron peaks in solution and in the film state. Besides, a stronger red-shift was observed in HFIP processed P (bgDPP-MeOT2) film, indicating stronger interchain interactions led by a more homogeneous film morphology (Fig. S1, ESI†). The comparison of absorption spectra between dry and swollen films (in 0.1 M NaCl) showed consistent results (Fig. S6, ESI†). For P(bgDPP-MeOT2) and P(lgDPP-MeOT2), both the main peaks have a slight blue-shift, possibly due to the entry of water breaking up the molecule packing, while there are negligible differences for P(bgDPP-T) and P(bgDPP-T2). In addition, we observed the polaron peaks of the two MeOT2 polymers in aqueous environment because they are susceptible to oxygen doping due to their high HOMO energy levels (Fig. S6, ESI†). Interestingly, P(lgDPP-MeOT2) with linear chains exhibited more redshifted absorption than P(bgDPP-MeOT2) with branched side chains. These results were further confirmed by CV measurements (Fig. S7, S8 and Table S2, ESI†). According to the ionization potentials (IPs) extracted from CV, DPP polymers with MeOT2 donor possess lower IPs of 4.62 eV for P(bgDPP-MeOT2) and 4.35 eV for P(lgDPP-MeOT2), suggesting that they are more susceptible to oxidation than P(bgDPP-T) and P(bgDPP-T2). DFT calculations showed that all the polymers exhibited planar backbones with small dihedral angles (Fig. 1b and Fig. S9, ESI†). Since linear side chains provide less interchain steric hindrance, we will prove later that P(lgDPP-MeOT2) has a closer molecular packing. This will lead to more planar backbones and enhanced interchain interactions, both of which will result in a smaller bandgap. Since the negligible spectrum difference after annealing the films and the unannealed films showed better device performance, all subsequent films were processed without further annealing.

Spectroelectrochemistry was used to evaluate the electrochemical activity of the DPP polymers, by virtue of its consecutive and controllable electrochemical doping under programmable bias conditions. The changes in absorption spectra and current density upon applying different potentials were monitored in 0.1 M NaCl aqueous solution. All polymers exhibited reversible and stable electrochemical redox features over 20 CV cycles (Fig. S8, ESI†). Gradually increasing the bias voltage from −0.2 to 0.6 V, three DPP polymers with different donors exhibited different electrochromic activities (Fig. 1c–f and Fig. S7, S8 and Fig. S10, S11, ESI†). Concretely, both P(bgDPP-T) and P(bgDPP-T2) exhibited a partial extinction of the π–π* absorption band (650–850 nm) and a gradually increased polaron absorption band (1000–1300 nm). It is notable that the absorption variations of P(bgDPP-T) and P(bgDPP-T2) at 750 nm and 1100 nm are not obvious until applied bias exceeds 0.3 V, higher than that (0.1 V) of P(bgDPP-MeOT2). To quantify the oxidation degree of the films during the electrochemical scan, differential spectra of DPP polymers were calculated to highlight the absorption variation by subtracting the spectrum of each film recorded under their neutral states (Fig. 1d, f and Fig. S11, ESI†).[35] Clearly, P(bgDPP-MeOT2) exhibited a more significant absorption variation in the π–π* absorption band (750–1050 nm) and the polaron absorption band (1050–1300 nm). These results indicate that P(bgDPP-MeOT2) is more liable to be p-doped in the aqueous environment. Similar results were also found in the linear chain polymer P(lgDPP-MeOT2), which is even more facile to be oxidized due to its increased HOMO energy level (Fig. S11, ESI†).

OECTs were fabricated using photolithography and parylene patterning methods according to the literature.[11,36] We

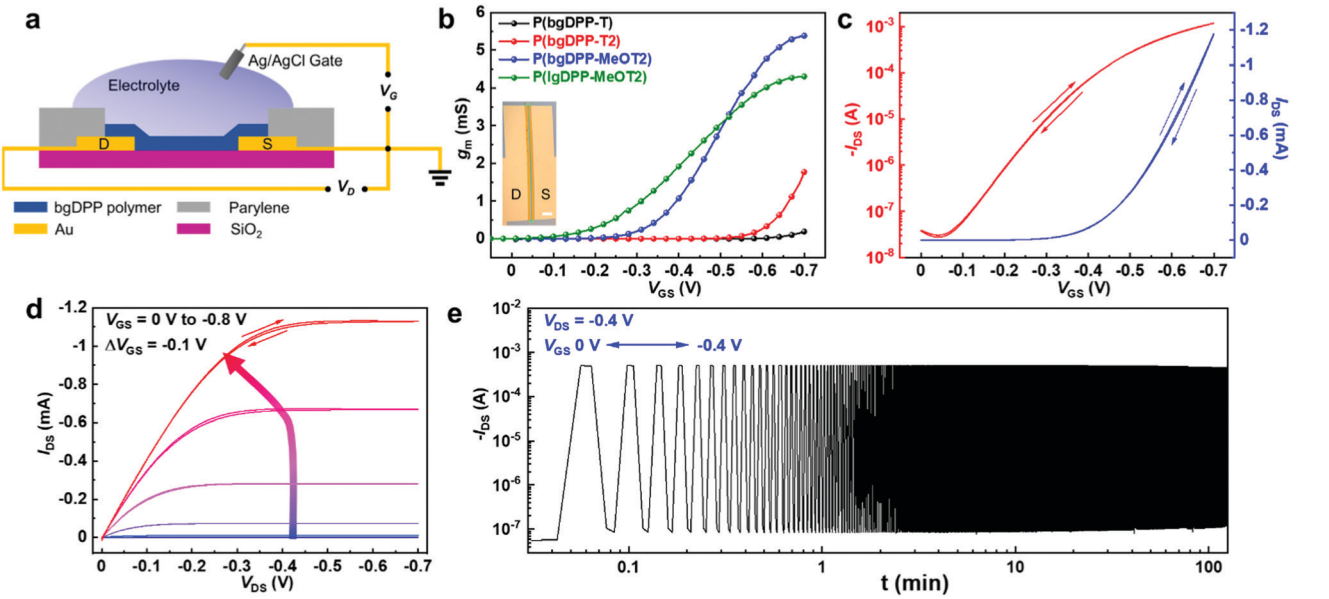

Fig. 2 OECT device structure and the device characteristics of P(bgDPP-MeOT2). (a) Schematic illustration of the OECT device structure in cross-section view and wiring diagram for device operation. (b) Transconductance curves of P(bgDPP-T), P(bgDPP-T2), P(lgDPP-MeOT2) and P(bgDPP-MeOT2). Inner photograph is the OECT channel with W/L of 1000/10 μm, scale bar: 100 μm. (c) Transfer and (d) output characteristics of P(bgDPP-MeOT2) OECTs. V_{DS} = −0.6 V. (e) Long-term on–off switching of P(bgDPP-MeOT2) operated with the indicated V_{DS}, V_{GS} values. Switching on time of V_{GS} and the interval time were both set to 2 s. All OECTs were measured in 0.1 M NaCl aqueous solution. W/L = 1000/10 μm in all devices. Film thickness d = 29.1 ± 0.8, 30.8 ± 1.7, 31.0 ± 1.3, 35.2 ± 1.7 nm for P(bgDPP-T), P(bgDPP-T2), P(lgDPP-MeOT2) and P(bgDPP-MeOT2), respectively.

explored many solvents for device fabrication, including *o*-DCB, chlorobenzene (CB), chloroform, 1,1,2,2-tetrachloroethane, and HFIP (Fig. S12, ESI†). We found that except for HFIP, other solvents cannot provide good device performance (g_m usually <0.1 mS for P(bgDPP-MeOT2)) using the spin-coating method. Only by employing the drop-casting method can a polymer solution using chloroform as the solvent exhibit similar device performance as that using HFIP; however, following with poor film uniformity. This is probably due to the strong aggregation of the D–A polymers in the solution state (Fig. S1, ESI†).[37] We have noticed that several papers also used drop-casting for device fabrication.[18,38] Hence, HFIP and the spin-coating were used for good film uniformity and reproducibility in this work. The figure of merit, μC^*, was extracted for performance comparison among different materials. All the DPP polymers exhibited typical p-type OECT behaviors and worked in accumulation mode (Fig. 2 and Fig. S13, ESI†). Among all the polymers, P(bgDPP-MeOT2) and P(lgDPP-MeOT2) with the strongest electron-donating moiety MeOT2, exhibited high g_m and high μC^* values (Table 1). P(bgDPP-MeOT2) exhibited the best OECT performance with a maximum transconductance of up to 5.33 mS with a film thickness of 64 nm, and high μC^* of up to 225 F cm^{-1} V^{-1} s^{-1}. P(bgDPP-MeOT2) showed negligible hysteresis during the forward and backward scans, suggesting its good and facile ion transport properties (Fig. 2c and d). With linear side chains, P(lgDPP-MeOT2) also exhibited outstanding OECT performance with high μC^* of 174 ± 25 F cm^{-1} V^{-1} s^{-1} (Fig. S13, ESI†). In contrast, P(bgDPP-T2) and P(bgDPP-T) showed inferior OECT performance with μC^* values of 42 ± 10 and 6 ± 1 F cm^{-1} V^{-1} s^{-1}. Thus, the electron-donating properties play an important role in the OECT performance of the DPP polymers. Notably, the polymer containing the MeOT2 moiety showed a lower threshold voltage (V_{Th}) compared to that containing T and T2 moieties. Interestingly, P(lgDPP-MeOT2) with linear side chains showed even lower V_{Th} (Fig. S15, ESI†). These results are consistent with the CV and spectroelectrochemistry studies. Besides, the molecular weight of polymers also strongly influences the OECT performance, since the P(bgDPP-MeOT2) with low M_w only show poor OECT performance with μC^* values of 0.12 F cm^{-1} V^{-1} s^{-1} (Fig. S16, ESI†). The criterion to judge whether a device works in the OECT mode or the electrolyte-gated organic field effect transistor (EGOFET) mode is the channel thickness dependence.[4,40] OECTs with different film thicknesses were also fabricated (Fig. S14, ESI†). Our devices showed clear film thickness dependent transconductance, suggesting that they indeed work in the OECT mode. P(bgDPP-MeOT2) and P(lgDPP-MeOT2) show high μC^* values, and the performance is both related to the molecular design and special processing solvent. We verified that HFIP is also good for performance enhancement in the polythiophene system (Table S4 and Fig. S17, ESI†). We believe that HFIP is likely to be more suitable for EG side-chain polymers than the solvents used for processing conventional alkyl side-chain polymers.

Stressing measurements upon continuous biasing and long-term on–off switching tests were performed to demonstrate the stable operation of P(bgDPP-MeOT2) statically and dynamically. The drain current of the P(bgDPP-MeOT2) devices stayed almost unchanged at low and moderate DC bias voltages, after continuous stress for 10 minutes, while higher biasing conditions only lead to a slight loss of ~1.7% on drain current ($V_{DS} = V_{GS} = -0.6$ V) (Fig. S18, ESI†). Moreover, long-term on–off switching cycle tests of P(bgDPP-MeOT2) were also monitored (Fig. 2e). The P(bgDPP-MeOT2) device exhibited good stability with a current retention of 98.8% for 700 switching cycles and 89% for over 3000 cycles (Fig. 2e and Fig. S19, ESI†), which is as good as the current state-of-the-art polythiophene based OECT channel materials.[17,19] Hence, P(bgDPP-MeOT2) also possesses outstanding stability upon continuous operation. To further understand the volumetric doping process of DPP polymers, the electrochemical impedance spectroscopy (EIS) technique was used. Spin-coated polymer films with certain areas and thicknesses on Au electrodes served as the working electrode with respect to Pt mesh as the counter electrode and Ag/AgCl pellet as the reference electrode. The effective capacitance could be extracted by fitting their EIS data *via* an equivalent circuit model ($R_s(R_p \| C)$), *i.e.* a capacitor (C) connects a resistor (R_p) in parallel and further a resistor (R_s) in series (Fig. 3b). The extracted capacitances of P(bgDPP-MeOT2) upon different channel volumes were plotted, exhibiting a good linear relationship with the channel volume (Fig. 3a). The volumetric capacitance (C^*) was extracted with a value of 120.0 ± 2.4 F cm^{-3}. With linear EG chains, P(lgDPP-MeOT2) showed a volumetric capacitance of 80.8 ± 1.4 F cm^{-3} (Fig. S20 (ESI†) and Table 1), lower than that of P(bgDPP-MeOT2). Based on the μC^* and C^* values, the hole mobility (μ) of both MeOT2 polymers can be calculated. P(bgDPP-MeOT2) showed a hole mobility of 1.63 ± 0.14 cm^2 V^{-1} s^{-1}, and P(lgDPP-MeOT2) showed a higher hole mobility of 2.15 ± 0.27 cm^2 V^{-1} s^{-1} (Table 1). The mobility values are very close to their alkyl side chain counterparts

Table 1 Summary of the OECTs performance and molecular packing for the DPP polymers[a]

Polymer	d[39 a]	$g_{m,max}$[a] [mS]	$I_{on/off}$	V_{Th}[b] [V]	μ[c] [cm^2 V^{-1} s^{-1}]	C^* [F cm^{-3}]	μC^*[d] [F cm^{-2} V^{-1} s^{-1}]	τ_{on} [μs]	τ_{off} [μs]	$d_{lamellar}$ [Å]	$d_{\pi-\pi}$ [Å]
P(bgDPP-T)	29.1 ± 0.8	0.019	2.2×10^3	−0.60	1.59 ± 0.15	3.7 ± 0.1	6 ± 1	—	—	22.7	3.57
P(bgDPP-T2)	72.5 ± 0.9	0.403	1.8×10^5	−0.57	0.50 ± 0.11	84.1 ± 1.5	42 ± 10	—	—	20.7	3.51
P(lgDPP-MeOT2)	60.9 ± 0.4	7.04	4.9×10^4	−0.17	2.15 ± 0.27	80.8 ± 1.4	174 ± 25	578	63	18.6	3.45
P(bgDPP-MeOT2)	64.1 ± 2.4	5.33	1.7×10^5	−0.33	1.63 ± 0.14	120.0 ± 2.4	195 ± 21	516	30	20.7	3.55

All the OECT devices were operated in a 0.1 M NaCl aqueous solution. [a] 14 devices with the same channel dimensions were tested and counted for each polymer (W/L = 100/10 μm), $V_{DS} = -0.6$ V. [b] The threshold voltage, V_{Th}, was determined by extrapolating the corresponding $I_{DS}^{1/2}$ *vs.* V_{GS} plots. [c] Charge carrier mobility μ was calculated from the μC^* and the measured volumetric capacitance C^*. [d] Materials' figure of merit μC^* was calculated from the measured transconductance.

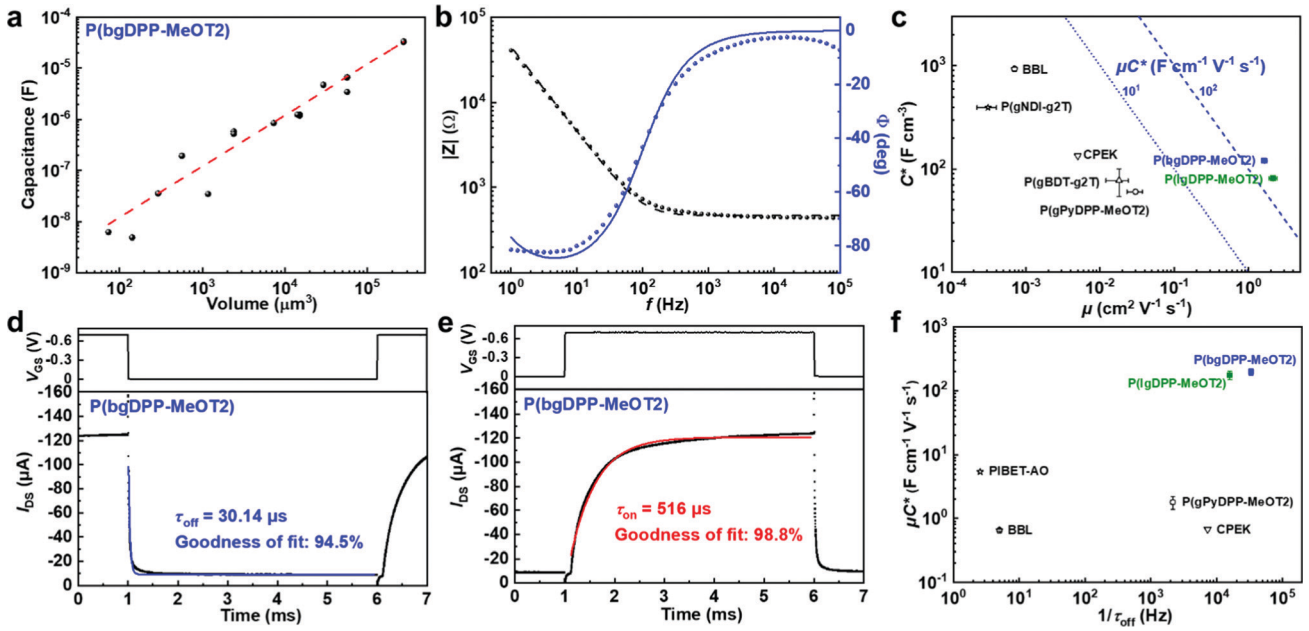

Fig. 3 Capacitive and transient behaviors of P(bgDPP-MeOT2). (a) Volume–capacitance relationship of P(bgDPP-MeOT2) was measured through the electrochemical impedance spectrum. The linear fit to the capacitance data is marked with a red dashed line. (b) The corresponding Bode and phase plot of P(bgDPP-MeOT2) with a channel area of 1 mm^2 and thickness of 56.8 ± 4.2 nm. Data fits were performed *via* the equivalent circuit of $R_s(R_p\|C)$. (c) Performance comparison *via* 2D μ–C^* plot for P(lgDPP-MeOT2), P(bgDPP-MeOT2), and other reported D–A polymer materials for OECTs.[21,28,30,38,41] (d and e) Off- and on-time constant of P(bgDPP-MeOT2) obtained by applying a gate voltage pulse with a time scale of 5 ms. Blue and red lines were fitted through exponential decay function. W/L = 100/10 μm and d = 34.8 ± 0.8 nm. (f) Performance comparison *via* 2D μC^*–$1/\tau_{off}$ plot for P(lgDPP-MeOT2), P(bgDPP-MeOT2), and other reported D–A polymer materials for OECTs.[21,27,30,41]

measured in OFETs.[33,42] In OFETs, after introducing linear side chains, the mobility will also increase, largely due to less steric hindrance at the branching positions and a closer π–π stacking distance.[43,44]

To evaluate the response speed of P(bgDPP-MeOT2), time constants during the turn-on and turn-off operation were both measured. As depicted in Fig. 3d and e, after applying a 5 ms pulse voltage on the Ag/AgCl gate, temporal responses of the drain current were recorded and fitted with the exponential decay function as described by the equation below,[12,17]

$$I_{DS}(t) = I_{DS,0} + a \times \exp(-t/\tau) \quad (2)$$

where $I_{DS}(t)$ represents the drain current at time t after applying the pulse gate bias, $I_{DS,0}$ represents the initial drain current before applying the pulse bias, a is a constant and τ is the time constant. The off-time constant (τ_{off}) and on-time constant (τ_{on}) were estimated to be 30 μs and 516 μs for P(bgDPP-MeOT2), with a channel geometry of 100 μm/10 μm (W/L). Obviously, both off- and on-time constants of P(bgDPP-MeOT2) reach the top-performing level among reported polymers, including D–A polymers and polythiophenes (Fig. 3f and Table S3, ESI†). According to the literature, the time constant of p-type OECT is mainly dominated by the ion injection process and the removal of holes from the source electrode.[12,36] Gaining a higher hole mobility or volumetric capacitance can effectively enhance the response speed. Specifically, P(lgDPP-MeOT2) also exhibited a fast response characteristic on the transient behaviours. On- and off-time constant of P(lgDPP-MeOT2) under a similar channel geometry achieved 578 μs and 63 μs, respectively (Fig. S21, ESI†). As discussed in the introduction part, both μC^* and response speed are important for OECTs. To more comprehensively compare the OECT performance, in Fig. 3f, we use both parameters to compare the materials' performances. It is obvious that P(bgDPP-MeOT2) and P(lgDPP-MeOT2) exhibit superior performances in both μC^* and switching speed.[17,18,27,36,45,46]

Crystallinity and molecular packing of conjugated polymers strongly influence water uptake, ion transport, and charge carrier transport in the polymer bulk. Two-dimensional grazing incidence wide angle X-ray scattering (2D-GIWAXS) was employed to reveal the differences between the polymers. All bgDPP polymers oriented preferably in a face-on fashion, while P(lgDPP-MeOT2) with linear EG chains, oriented predominantly with edge-on (Fig. 4 and Fig. S22, ESI†). P(lgDPP-MeOT2) exhibited a closer π–π stacking distance of 3.45 Å, smaller than those of the bgDPP polymers (3.51–3.57 Å) (Fig. S19, ESI†), consisting with our previous absorption spectra analysis and mobility results. In addition, P(lgDPP-MeOT2) also exhibited three orders of lamellar scattering peaks, (100), (200), and (300), indicating the well-packed polymer side chains compared with those with branched side chains. For conjugated polymers with highly ordered crystallites, the injection of hydrated ions into polymer bulk may induce the destruction of the morphology and then impede charge transport between adjacent crystallites.[15,47] Therefore, less ordered packing of P(bgDPP-MeOT2) might contribute to the enhanced

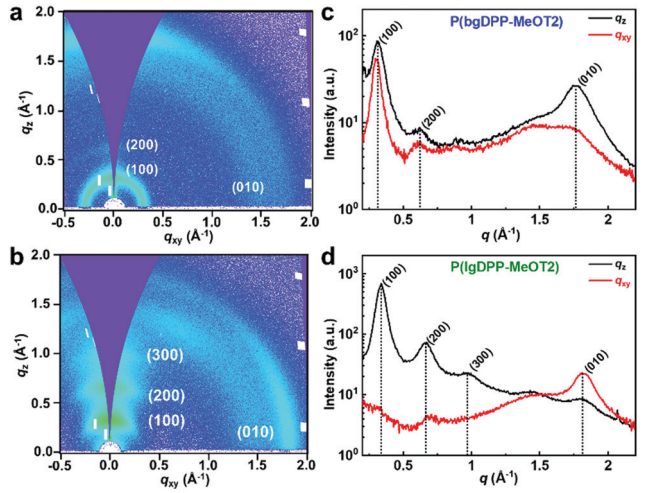

Fig. 4 2D-GIWAXS patterns of (a) P(bgDPP-MeOT2) and (b) P(lgDPP-MeOT2). (c and d) The corresponding line cuts of P(bgDPP-MeOT2) and P(lgDPP-MeOT2). Cuts along the q_{xy} direction (red) represent scattering in the plane of the substrate, while the scattering in the q_z direction (black) results from out-of-plane scattering.

penetration of hydrated ions into the polymer bulk (higher C^*) and faster temporal response, though its hole mobility is slightly sacrificed.

Conclusions

In conclusion, we have systematically explored the influences of the donor, side chain, molecular weight, and processing conditions to solve the low-performance issue of D–A conjugated polymers. The high-performance of P(bgDPP-MeOT2) can be attributed to the following molecular design and device fabrication considerations: (i) the strong electron-donating moiety MeOT2 reduces the ionization potential of DPP polymers, leading to a low threshold voltage and high volumetric capacitance; (ii) the branched EG chains guarantee enough solubility for high molecular weight polymers and also facilitate ion injection/ejection in the polymer bulk; (iii) optimized polymerization conditions allow comparable molecular weight and hole mobility to its alkyl side chain counterpart; and (iv) a polar solvent HFIP is used to disaggregate the polymers for better film quality. These efforts lead to high μC^* (>200 F cm^{-1} V^{-1} s^{-1}), high hole mobility (>1.6 cm^2 V^{-1} s^{-1}), and fast response (τ_{off} 30 μs; τ_{on} 516 μs), among the highest of OECT materials (Table S3, ESI†). Interestingly, we come to a distinct conclusion compared to the recent work by McCulloch *et al.*,[31] further revealing the complexity of D–A polymers. More factors including the synthetic method, side-chain engineering, and processing conditions, need to be carefully considered for obtaining high-performance OECTs. We believe this systematic study will provide a guidance for the future study of other OMIEC materials.

Conflicts of interest

There are no conflicts to declare.

Acknowledgements

This work is supported by the National Natural Science Foundation of China (22075001), the Key-Area Research and Development Program of Guangdong Province (2019B010934001), the Open Fund of the State Key Laboratory of Luminescent Materials and Devices (South China University of Technology, 2021-skllmd-02), and the Beijing Natural Science Foundation (2192020). T. L. thanks the Clinical Medicine Plus X – Young Scholars Project, Peking University, the Fundamental Research Funds for the Central Universities. S. Z., Y. W., and X. G. thank the U.S. Department of Energy, Office of Science, Office of Basic Energy Science (SC0019361). The computational part is supported by High-Performance Computing Platform of Peking University.

References

1 J. Rivnay, R. M. Owens and G. G. Malliaras, *Chem. Mater.*, 2013, **26**, 679.
2 B. D. Paulsen, K. Tybrandt, E. Stavrinidou and J. Rivnay, *Nat. Mater.*, 2020, **19**, 13.
3 G. D. Spyropoulos, J. N. Gelinas and D. Khodagholy, *Sci. Adv.*, 2019, **5**, eaau7378.
4 J. Rivnay, P. Leleux, M. Ferro, M. Sessolo, A. Williamson, D. A. Koutsouras, D. Khodagholy, M. Ramuz, X. Strakosas, R. M. Owens, C. Benar, J. M. Badier, C. Bernard and G. G. Malliaras, *Sci. Adv.*, 2015, **1**, e1400251.
5 V. Venkatraman, J. T. Friedlein, A. Giovannitti, I. P. Maria, I. McCulloch, R. R. McLeod and J. Rivnay, *Adv. Sci.*, 2018, **5**, 1800453.
6 O. Parlak, S. T. Keene, A. Marais, V. F. Curto and A. Salleo, *Sci. Adv.*, 2018, **4**, eaar2904.
7 A. M. Pappa, D. Ohayon, A. Giovannitti, I. P. Maria, A. Savva, I. Uguz, J. Rivnay, I. McCulloch, R. M. Owens and S. Inal, *Sci. Adv.*, 2018, **4**, eaat0911.
8 P. Li, T. Lei and L. Ding, *Sci. Bull.*, 2020, **65**, 1141.
9 Y. van de Burgt, E. Lubberman, E. J. Fuller, S. T. Keene, G. C. Faria, S. Agarwal, M. J. Marinella, A. Alec Talin and A. Salleo, *Nat. Mater.*, 2017, **16**, 414.
10 Y. van de Burgt, A. Melianas, S. T. Keene, G. Malliaras and A. Salleo, *Nat. Electron.*, 2018, **1**, 386.
11 S. Inal, G. G. Malliaras and J. Rivnay, *Nat. Commun.*, 2017, **8**, 1767.
12 D. A. Bernards and G. G. Malliaras, *Adv. Funct. Mater.*, 2007, **17**, 3538.
13 D. Khodagholy, T. Doublet, P. Quilichini, M. Gurfinkel, P. Leleux, A. Ghestem, E. Ismailova, T. Herve, S. Sanaur, C. Bernard and G. G. Malliaras, *Nat. Commun.*, 2013, **4**, 1575.
14 P. Gkoupidenis, N. Schaefer, B. Garlan and G. G. Malliaras, *Adv. Mater.*, 2015, **27**, 7176.
15 R. Giridharagopal, L. Q. Flagg, J. S. Harrison, M. E. Ziffer, J. Onorato, C. K. Luscombe and D. S. Ginger, *Nat. Mater.*, 2017, **16**, 737.

16 C. Cea, G. D. Spyropoulos, P. Jastrzebska-Perfect, J. J. Ferrero, J. N. Gelinas and D. Khodagholy, *Nat. Mater.*, 2020, **19**, 679.
17 A. Giovannitti, D. T. Sbircea, S. Inal, C. B. Nielsen, E. Bandiello, D. A. Hanifi, M. Sessolo, G. G. Malliaras, I. McCulloch and J. Rivnay, *Proc. Natl. Acad. Sci. U. S. A.*, 2016, **113**, 12017.
18 C. B. Nielsen, A. Giovannitti, D. T. Sbircea, E. Bandiello, M. R. Niazi, D. A. Hanifi, M. Sessolo, A. Amassian, G. G. Malliaras, J. Rivnay and I. McCulloch, *J. Am. Chem. Soc.*, 2016, **138**, 10252.
19 M. Moser, T. C. Hidalgo, J. Surgailis, J. Gladisch, S. Ghosh, R. Sheelamanthula, Q. Thiburce, A. Giovannitti, A. Salleo, N. Gasparini, A. Wadsworth, I. Zozoulenko, M. Berggren, E. Stavrinidou, S. Inal and I. McCulloch, *Adv. Mater.*, 2020, **32**, e2002748.
20 S. M. Kim, C. H. Kim, Y. Kim, N. Kim, W. J. Lee, E. H. Lee, D. Kim, S. Park, K. Lee, J. Rivnay and M. H. Yoon, *Nat. Commun.*, 2018, **9**, 3858.
21 H. Sun, M. Vagin, S. Wang, X. Crispin, R. Forchheimer, M. Berggren and S. Fabiano, *Adv. Mater.*, 2018, **30**, 1704916.
22 M. Kawan, T. C. Hidalgo, W. Du, A.-M. Pappa, R. M. Owens, I. McCulloch and S. Inal, *Mater. Horiz.*, 2020, **7**, 2348.
23 J. Yang, Z. Y. Zhao, S. Wang, Y. L. Guo and Y. Q. Liu, *Chem*, 2018, **4**, 2748.
24 H. Jia and T. Lei, *J. Mater. Chem. C*, 2019, **7**, 12809.
25 X. Yan, M. Xiong, J. T. Li, S. Zhang, Z. Ahmad, Y. Lu, Z. Y. Wang, Z. F. Yao, J. Y. Wang, X. Gu and T. Lei, *J. Am. Chem. Soc.*, 2019, **141**, 20215.
26 S. Fratini, M. Nikolka, A. Salleo, G. Schweicher and H. Sirringhaus, *Nat. Mater.*, 2020, **19**, 491.
27 Y. Wang, E. Zeglio, H. Liao, J. Xu, F. Liu, Z. Li, I. P. Maria, D. Mawad, A. Herland, I. McCulloch and W. Yue, *Chem. Mater.*, 2019, **31**, 9797.
28 A. Giovannitti, C. B. Nielsen, D. T. Sbircea, S. Inal, M. Donahue, M. R. Niazi, D. A. Hanifi, A. Amassian, G. G. Malliaras, J. Rivnay and I. McCulloch, *Nat. Commun.*, 2016, **7**, 13066.
29 A. Giovannitti, I. P. Maria, D. Hanifi, M. J. Donahue, D. Bryant, K. J. Barth, B. E. Makdah, A. Savva, D. Moia, M. Zetek, P. R. F. Barnes, O. G. Reid, S. Inal, G. Rumbles, G. G. Malliaras, J. Nelson, J. Rivnay and I. McCulloch, *Chem. Mater.*, 2018, **30**, 2945.
30 A. Giovannitti, R. B. Rashid, Q. Thiburce, B. D. Paulsen, C. Cendra, K. Thorley, D. Moia, J. T. Mefford, D. Hanifi, D. Weiyuan, M. Moser, A. Salleo, J. Nelson, I. McCulloch and J. Rivnay, *Adv. Mater.*, 2020, **32**, e1908047.
31 M. Moser, A. Savva, K. Thorley, B. D. Paulsen, T. C. Hidalgo, D. Ohayon, H. Chen, A. Giovannitti, A. Marks, N. Gasparini, A. Wadsworth, J. Rivnay, S. Inal and I. McCulloch, *Angew. Chem., Int. Ed.*, 2021, **60**, 7777.
32 B. Carsten, F. He, H. J. Son, T. Xu and L. Yu, *Chem. Rev.*, 2011, **111**, 1493.
33 R. Di Pietro, T. Erdmann, J. H. Carpenter, N. Wang, R. R. Shivhare, P. Formanek, C. Heintze, B. Voit, D. Neher, H. Ade and A. Kiriy, *Chem. Mater.*, 2017, **29**, 10220.
34 A. Giovannitti, I. P. Maria, D. Hanifi, M. J. Donahue, D. Bryant, K. J. Barth, B. E. Makdah, A. Savva, D. Moia, M. Zetek, P. R. F. Barnes, O. G. Reid, S. Inal, G. Rumbles, G. G. Malliaras, J. Nelson, J. Rivnay and I. McCulloch, *Chem. Mater.*, 2018, **30**, 2945.
35 P. Schmode, D. Ohayon, P. M. Reichstein, A. Savva, S. Inal and M. Thelakkat, *Chem. Mater.*, 2019, **31**, 5286.
36 D. Khodagholy, J. Rivnay, M. Sessolo, M. Gurfinkel, P. Leleux, L. H. Jimison, E. Stavrinidou, T. Herve, S. Sanaur, R. M. Owens and G. G. Malliaras, *Nat. Commun.*, 2013, **4**, 2133.
37 M. Li, H. Bin, X. Jiao, M. M. Wienk, H. Yan and R. A. J. Janssen, *Angew. Chem., Int. Ed.*, 2020, **59**, 846.
38 A. Giovannitti, K. J. Thorley, C. B. Nielsen, J. Li, M. J. Donahue, G. G. Malliaras, J. Rivnay and I. McCulloch, *Adv. Funct. Mater.*, 2018, **28**, 1706325.
39 J. Qiu, T. Yu, W. Zhang, Z. Zhao, Y. Zhang, G. Ye, Y. Zhao, X. Du, X. Liu, L. Yang, L. Zhang, S. Qi, Q. Tan, X. Guo, G. Li, S. Guo, H. Sun, D. Wei and N. Liu, *ACS Mater. Lett.*, 2020, **2**, 999.
40 E. Zeglio and O. Inganas, *Adv. Mater.*, 2018, **30**, e1800941.
41 A. T. Lill, D. X. Cao, M. Schrock, J. Vollbrecht, J. Huang, T. Nguyen-Dang, V. V. Brus, B. Yurash, D. Leifert, G. C. Bazan and T. Q. Nguyen, *Adv. Mater.*, 2020, **32**, e1908120.
42 Y. Li, P. Sonar, S. P. Singh, M. S. Soh, M. van Meurs and J. Tan, *J. Am. Chem. Soc.*, 2011, **133**, 2198.
43 T. Lei, J. H. Dou and J. Pei, *Adv. Mater.*, 2012, **24**, 6457.
44 Z. Wang, Z. Liu, L. Ning, M. Xiao, Y. Yi, Z. Cai, A. Sadhanala, G. Zhang, W. Chen, H. Sirringhaus and D. Zhang, *Chem. Mater.*, 2018, **30**, 3090.
45 A. Savva, R. Hallani, C. Cendra, J. Surgailis, T. C. Hidalgo, S. Wustoni, R. Sheelamanthula, X. Chen, M. Kirkus, A. Giovannitti, A. Salleo, I. McCulloch and S. Inal, *Adv. Funct. Mater.*, 2020, **30**, 1907657.
46 S. Inal, J. Rivnay, P. Leleux, M. Ferro, M. Ramuz, J. C. Brendel, M. M. Schmidt, M. Thelakkat and G. G. Malliaras, *Adv. Mater.*, 2014, **26**, 7450.
47 L. Q. Flagg, C. G. Bischak, J. W. Onorato, R. B. Rashid, C. K. Luscombe and D. S. Ginger, *J. Am. Chem. Soc.*, 2019, **141**, 4345.

